Article

Determination of the Rod–Wire Transition Length in Colloidal Indium Phosphide Quantum Rods

Fudong Wang, and William E. Buhro

J. Am. Chem. Soc., **2007**, 129 (46), 14381-14387• DOI: 10.1021/ja075015c • Publication Date (Web): 30 October 2007

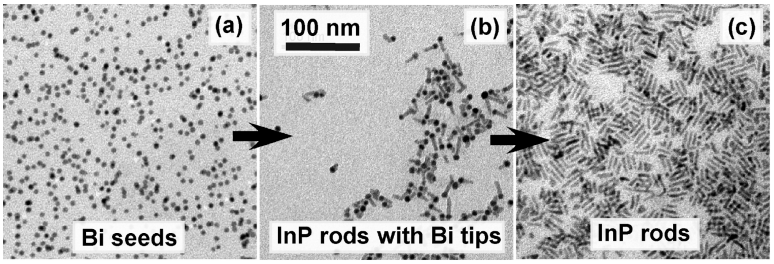

More About This Article

Additional resources and features associated with this article are available within the HTML version:

- Supporting Information
- Links to the 10 articles that cite this article, as of the time of this article download
- Access to high resolution figures
- Links to articles and content related to this article
- Copyright permission to reproduce figures and/or text from this article

View the Full Text HTML

J|A|C|S
ARTICLES
Published on Web 10/30/2007

Determination of the Rod−Wire Transition Length in Colloidal Indium Phosphide Quantum Rods

Fudong Wang and William E. Buhro*

Contribution from the Department of Chemistry and Center for Materials Innovation, Washington University, St. Louis, Missouri 63130-4899

Received July 6, 2007; E-mail: buhro@wustl.edu

Abstract: Colloidal InP quantum rods (QRs) having controlled diameters and lengths are grown by the solution−liquid−solid method, from Bi nanoparticles in the presence of hexadecylamine and other conventional quantum dot surfactants. These quantum rods show band-edge photoluminescence after HF photochemical etching. Photoluminescence efficiency is further enhanced after the Bi tips are selectively removed from the QRs by oleic acid etching. The QRs are anisotropically 3D confined, the nature of which is compared to the corresponding isotropic 3D confinement in quantum dots and 2D confinement in quantum wires. The 3D−2D rod−wire transition length is experimentally determined to be 25 nm, which is about 2 times the bulk InP exciton Bohr radius (of ∼11 nm).

Introduction

Semiconductor quantum rods (QRs) exist within the transitional regime between 3D-confined quantum dots (QDs) and 2D-confined quantum wires (QWs).[1,2] They are anisotropically 3D confined and exhibit both diameter- and length-dependent optical properties.[3,4] The length at which the third dimension of confinement in QRs becomes fully relaxed such that they acquire the 2D confinement of QWs is not fully understood. Theoretical studies of CdSe QRs suggested that the third confinement dimension disappears in QRs longer than approximately twice the bulk exciton Bohr radius (which is 5.6 nm in CdSe).[5,6] An experimental study by Banin and co-workers found that the band gap in CdSe QRs showed no significant dependence on rod length for lengths longer than 11 nm, in agreement with the theoretical results.[7] However, a separate analysis of experimental data from Alivisatos and co-workers found that CdSe QRs achieved 2D confinement at lengths of ca. ≥30 nm, or approximately 6 times the Bohr radius.[2] To date, the 3D−2D transition lengths in III−V QRs have not been determined. Because of the generally larger exciton Bohr radii in III−V semiconductors, and consequently larger confinement effects, the 3D−2D transition should occur at longer lengths in III−V QRs than in II−VI QRs. Determining that transition length in InP QRs and comparing it to the bulk exciton Bohr radius of 11 nm is a major goal of this work.

QRs exhibit potential technological advantages over QDs in applications such as lasers,[8] light-harvesting (photovoltaic) cells,[9] linearly polarized emission,[3,10] and their propensity to form liquid crystalline phases.[11] From the perspectives of both fundamental studies and technical applications, shape-controlled synthesis of high-quality QRs having narrow diameter and length distributions is highly desirable. Shape-controlled growth of nanocrystals remains one of the most important challenges in nanoscience.

Research on the synthesis of colloidal QRs has focused largely on wurtzite II−VI semiconductor systems,[4,12−19] where the surfactant-controlled growth approach has been demonstrated.[12−17] Anisotropic growth at high monomer concentrations is believed to result from variations in growth rates along different crystallographic directions because of differential binding of surfactants to different crystal faces. Syntheses of colloidal III−V QRs are less advanced, with complications arising from the higher symmetry of the zinc blende crystal structure, higher covalent character, and less-available precursors.[20,21] Preparation

(1) Buhro, W. E.; Colvin, V. L. *Nat. Mater.* **2003**, *2*, 138−139.
(2) Yu, H.; Li, J.; Loomis, R. A.; Gibbons, P. C.; Wang, L.-W.; Buhro, W. E. *J. Am. Chem. Soc.* **2003**, *125*, 16168−16169.
(3) Kan, S.; Mokari, T.; Rothenberg, E.; Banin, U. *Nat. Mater.* **2003**, *2*, 155−158.
(4) Li, L.-S.; Hu, J.; Yang, W.; Alivisatos, A. P. *Nano Lett.* **2001**, *1*, 349−351.
(5) Hu, J.; Wang, L.-W.; Li, L.-S.; Yang, W.; Alivisatos, A. P. *J. Phys. Chem. B* **2002**, *106*, 2447−2452.
(6) Li, J.; Wang, L.-W. *Nano Lett.* **2003**, *3*, 101−105.
(7) Katz, D.; Wizansky, T.; Millo, O.; Rothenberg, E.; Mokari, T.; Banin, U. *Phys. Rev. Lett.* **2002**, *89*, 086801.
(8) Kazes, M.; Lewis, D. Y.; Ebenstein, Y.; Mokari, T.; Banin, U. *Adv. Mater.* **2002**, *14*, 317−321.
(9) Huynh, W. U.; Dittmer, J. J.; Alivisatos, A. P. *Science* **2002**, *295*, 2425−2427.
(10) Hu, J.; Li, L.-S.; Yang, W.; Manna, L.; Wang, L.-W.; Alivisatos, A. P. *Science* **2001**, *292*, 2060−2063.
(11) Li, L.-S.; Walda, J.; Manna, L.; Alivisatos, A. P. *Nano Lett.* **2002**, *2*, 557−560.
(12) Peng, X.; Manna, L.; Yang, W.; Wickham, J.; Scher, E.; Kadavanich, A.; Alivisatos, A. P. *Nature* **2000**, *404*, 59−61.
(13) Yu, W. W.; Wang, Y. A.; Peng, X. *Chem. Mater.* **2003**, *15*, 4300−4308.
(14) Manna, L.; Scher, E. C.; Alivisatos, A. P. *J. Am. Chem. Soc.* **2000**, *122*, 12700−12706.
(15) Peng, Z. A.; Peng, X. *J. Am. Chem. Soc.* **2001**, *123*, 1389−1395.
(16) Peng, Z. A.; Peng, X. *J. Am. Chem. Soc.* **2002**, *124*, 3343−3353.
(17) Peng, X. *Adv. Mater.* **2003**, *15*, 459−463.
(18) Manna, L.; Scher, E. C.; Li, L.-S.; Alivisatos, A. P. *J. Am. Chem. Soc.* **2002**, *124*, 7136−7145.
(19) Mokari, T.; Banin, U. *Chem. Mater.* **2003**, *15*, 3955−3960.
(20) Battaglia, D.; Peng, X. *Nano Lett.* **2002**, *2*, 1027−1030.
(21) Kim, Y.-H.; Jun, Y.-W.; Jun, B.-H.; Lee, S.-M.; Cheon, J. *J. Am. Chem. Soc.* **2002**, *124*, 13656−13657.

of InAs[3,22] and InP QRs[23−25] by the solution−liquid−solid (SLS) mechanism[26] has been separately demonstrated by Banin and co-workers and Mićić and co-workers, where metallic nanoparticles preformed or generated in situ catalyzed the anisotropic growth of rods. However, III−V QRs have not been obtained over a sufficiently large diameter range for systematic study of the diameter dependence of the band gap, or over a sufficient length range to identify the 3D−2D transition length.

In this article, we demonstrate the SLS growth of soluble, narrowly dispersed InP QRs with controlled diameters and lengths, using near-monodispersed colloidal Bi nanoparticles as catalysts and hexadecylamine (HDA) and other conventional QD surfactants as stabilizers. The diameters of InP QRs were mainly dependent on the diameters of Bi nanoparticles employed, whereas the lengths were determined by the reaction time. The Bi nanoparticles present at one end of the rods were selectively removed, and the absorption spectra of like QRs with and without the Bi tips were compared. No detectable changes were observed, indicating that the Bi tips did not influence the absorption properties of the InP QRs. The as-synthesized, nonemissive InP QRs exhibited band-edge photoluminescence (PL) after photochemical etching with HF.[27] The PL efficiency was further enhanced when the Bi tips were removed, indicating partial PL quenching by the Bi tips. We further compared the quantum confinement of InP QDs, QRs, and QWs and determined that the InP QRs acquire the 2D confinement of QWs at lengths ≥25 nm, which is roughly twice the bulk exciton Bohr radius. InAs QRs with narrowly dispersed diameters and lengths were grown similarly using either near-monodispersed Bi or In nanoparticles.

Experimental Section

Materials. The precursor tris(trimethylsilyl)phosphine ($P(SiMe_3)_3$) was prepared by a literature method.[28] Stock solutions of $P(SiMe_3)_3$ (containing 0.40−0.42 mmol $P(SiMe_3)_3$/mL polydecene) were prepared and stored in a refrigerator for later use. The preparation of the indium myristate ($In(myr)_3$) stock solution was described elsewhere.[29] The Bi nanoparticle stock solutions (containing 0.04 mmol Bi atoms/g of solution) were prepared as previously described (method B);[2] the general synthetic procedure is also described in the Supporting Information. Tri-*n*-octylphosphine (TOP, 90%), dioctylamine (DOA, 98%), HDA (90%), tri-*n*-octylphosphine oxide (TOPO, 90%), oleic acid (OA, 90%), and hydrogenated poly(1-decene) were purchased from Aldrich. HDA and TOPO were vacuum distilled at 200 °C. Other reagents were used as received.

Synthesis of InP QRs. All synthetic procedures were conducted under dry, O_2-free N_2 (g), but the isolation and purification steps were conducted in the ambient atmosphere. The quantities of reagents and reaction conditions used are recorded in Table S1 (Supporting Information). In a typical preparation, the $In(myr)_3$ stock solution (1.65 g, 0.25 mmol of In), HDA (570 mg, 2.36 mmol), TOP (90 mg, 0.24 mmol), TOPO (250 mg, 0.65 mmol), and polydecene (3 g) were loaded into a Schlenk reaction tube. In a separate vial, the Bi nanoparticle stock solution (140−200 mg, 0.0056−0.008 mmol Bi atoms) and DOA (30 mg, 0.12 mmol) (in some experiments) were diluted with polydecene to 0.5 mL, and the vial was septum capped. The $P(SiMe_3)_3$ stock solution (0.5 mL, 0.20−0.21 mmol $P(SiMe_3)_3$) was loaded into a syringe. The reaction mixture in the Schlenk tube was degassed under vacuum (10^{-3} torr) at ∼100 °C for 5 min, then inserted into a preheated salt bath ($NaNO_3/KNO_3$, 46:54 by weight), held at a desired temperature (238−266 °C; Table S1). The tube was allowed to equilibrate for 1−2 min, and then the $P(SiMe_3)_3$ stock solution was quickly injected into the tube. The color of the reaction mixture immediately turned bright yellowish red. At a desired time (Table S1), the mixture containing Bi nanoparticles was quickly injected into the tube by a syringe. A brown to grayish olive color resulted in about 30 s. The tube was withdrawn from the bath at a desired time (total reaction time 0.5−3 min) and allowed to cool to room temperature. The $P(SiMe_3)_3$ stock solution and Bi nanoparticle mixture were injected together in the same syringe in some experiments, but generally they yielded slightly broader size distributions.

The InP QRs were isolated as a gel-like precipitate from the reaction mixture by adding toluene (ca. 2 mL) and 2-propanol (ca. 3 mL), followed by centrifugation (benchtop centrifuge) and decanting of the supernatant. The precipitate was redispersed in a mixture of toluene (ca. 3 mL) and 2-propanol (ca. 5 mL) upon sonication in a cleaning bath. The QRs were collected as a black precipitate by adding methanol (ca. 1 mL), followed by centrifugation and decanting of the supernatant. This redispersion−centrifugation purification process was repeated an additional time in a mixture of toluene (ca. 2 mL), 2-propanol (ca. 4 mL), and methanol (ca. 2 mL). The finally collected QRs were redispersed in toluene upon sonication to form a uniform and optically clear light brown solution for spectroscopic and TEM analyses. The absorption spectra showed no changes after such samples were allowed to stand for a few weeks in capped cuvettes.

Removal of Bi Nanoparticles from InP QRs. To the toluene solution (ca. 3 mL) of the purified InP QRs (whole batch) was added OA (250−800 mg, 0.89−2.83 mmol), and the mixture was sonicated in a cleaning bath at room temperature (the temperature generally increased to ∼50 °C because of heat generated by sonication). The amount of OA and the duration of etching are listed in Table S2. Typically, more OA and longer times were used when larger Bi nanoparticles were employed initially in the synthesis. The Bi tips could be removed within 6−8 h of sonication. The insoluble impurities in the solution were isolated and removed as a precipitate by centrifugation. The QRs in the supernatant were precipitated by adding methanol (ca. 5 mL), followed by centrifugation and decanting of the supernatant. The isolated QRs were redispersed in toluene for subsequent spectroscopic and TEM analyses. To narrow the length distributions, size-selective precipitation was performed by carefully adding methanol to the QR supernatant (after the insoluble impurities were removed) until the solution became a little cloudy, followed by centrifugation. The precipitate was the first fraction having longer QRs. The supernatant containing shorter QRs could be further subjected to the size-selective precipitation process. The slightly thinner rods could be obtained by employing further etching with OA (Tables S1 and S2).

HF Photochemical Etching of InP QRs. The etching experiments were performed in air in 30-mL transparent Nalgene Teflon FEP bottles using a modified literature method.[27] The HF etching solution (2.40 M) was prepared by diluting HF (1.065 g, 50 wt.%) in a mixture of *n*-butyl alcohol (10 mL) and water (140 mg). InP QRs constituting the entire batch from a single preparation were dispersed in toluene (3 mL), combined with *n*-butyl alcohol (9 mL), isooctane (3 mL), and TOPO (300−500 mg, 0.8−1.3 mmol). The HF etching solution (0.2−0.5 mL) was then added with stirring, and the mixture was exposed to the 300-W xenon lamp (1−2 h). The lamp was equipped with a long-pass filter

(22) Kan, S.; Aharoni, A.; Mokari, T.; Banin, U. *Faraday Discuss.* **2004**, *125*, 23−38.
(23) Ahrenkiel, S. P.; Mićić, O. I.; Miedaner, A.; Curtis, C. J.; Nedeljković, J. M.; Nozik, A. J. *Nano Lett.* **2003**, *3*, 833−837.
(24) Nedeljković, J. M.; Mićić, O. I.; Ahrenkiel, S. P.; Miedaner, A.; Nozik, A. J. *J. Am. Chem. Soc.* **2004**, *126*, 2632−2639.
(25) Shweky, I.; Aharoni, A.; Mokari, T.; Rothenberg, E.; Nadler, M.; Popov, I.; Banin, U. *Mater. Sci. Eng., C* **2006**, *26*, 788−794.
(26) Wang, F.; Dong, A.; Sun, J.; Tang, R.; Yu, H.; Buhro, W. E. *Inorg. Chem.* **2006**, *45*, 7511−7521.
(27) Talapin, D. V.; Gaponik, N.; Borchert, H.; Rogach, A.; Haase, M.; Weller, H. *J. Phys. Chem. B* **2002**, *106*, 12659−12663.
(28) Askham, F. R.; Stanley, G. C.; Marques, E. C. *J. Am. Chem. Soc.* **1985**, *107*, 7423−7431.
(29) Wang, F.; Yu, H.; Li, J.; Hang, Q.; Zemlyanov, D.; Gibbons, P. C.; Wang, L.-W.; Janes, D. B.; Buhro, W. E. *J. Am. Chem. Soc.* **2007**, *129*, 14327−14335.

having a cutoff wavelength of 700 nm. The QRs were then isolated as a precipitate by addition of CH_3CN (3 mL), followed by centrifugation and decanting of the supernatant. The isolated QRs were redispersed in toluene for subsequent spectroscopic and TEM analyses.

Results

Synthesis of InP QRs. The InP QRs were grown from Bi nanoparticles in polydecene (boiling point > 315 °C) using $P(SiMe_3)_3$ and $In(myr)_3$ (eq 1 and Table S1). The reaction mixtures contained conventional QD surfactants such as HDA, TOPO, and TOP to manipulate the growth of InP QRs. Addition of DOA to the Bi solution further protected Bi nanoparticles from agglomeration at high temperatures. The optimal $In(myr)_3$/$P(SiMe_3)_3$ molar ratio was 1.1−1.2, and the Bi/$P(SiMe_3)_3$ molar ratio was 24−36. The optimal HDA/TOPO/TOP/myristate molar ratio was 10/3/1/3.

$$\mathrm{In(myristate)_3} + \mathrm{P(SiMe_3)_3} \xrightarrow[\substack{\text{Bi nanoparticles}\\ \text{HDA, TOPO, TOP, (DOA)}}]{\text{238−266 °C, polydecene solvent}} \text{InP QRs} \quad (1)$$

The synthesis of InP QRs was conducted under conditions quite similar to those employed for the growth of InP QWs,[29] except for a few important differences. First, 1-octylphosphonic acid, which was essential to the growth of InP QWs,[29] was omitted in the QR synthesis. Second, the Bi nanoparticle/InP precursor ratio was increased by 2−3 times to limit the nanostructure growth to rod lengths. Third, the reaction time was kept short to also limit growth to rod lengths.

Figure 1 shows representative TEM images of the InP QRs. The Bi nanoparticles can be identified at one end of the QRs, confirming the SLS growth mechanism.[26] Most of the QRs were straight, although some of them were kinked (Figure S1). Statistical analysis conducted using TEM images revealed that the QRs had mean diameters of 4.2−7.8 nm and mean lengths of 10−39 nm excluding the Bi tips (see Figure S2 for representative size distribution histograms). The standard deviations in the diameter distributions ranged from 10 to 17% of the mean diameter, demonstrating that the QR specimens approached monodispersity in that dimension. The standard deviations in the length distributions ranged from 24 to 44% of the mean length, which were broad, but were narrowed by length-selective etching or precipitation upon removal of the Bi nanoparticles (see below).

The diameters of the QRs (d_{rod}) depended mainly on the diameters of the Bi nanoparticles (d_{cat}) used in their growth (Figure S3). The relationship between d_{rod} and d_{cat} was empirically fitted to the linear expression in eq 2. The lengths of the QRs depended on the reaction time (Table S1).

$$d_{rod}[\mathrm{nm}] = (0.43 \pm 0.03)d_{cat}[\mathrm{nm}] + (1.66 \pm 0.24) \quad (2)$$

A representative high-resolution TEM (HRTEM) image of a single rod (Figure 1f) established that the InP QRs exhibited the zinc blende structure of bulk InP and grew in the [111] orientation. X-ray powder diffraction of the QR specimens (Figure 2a) confirmed that the QRs had the zinc blende structure of bulk InP. Twin defects were observed for some rods, with the {111} twin planes oriented either 19° with respect to or perpendicular to the [111] growth direction (Figure S4). Energy dispersive X-ray (EDX) spectroscopy indicated an average composition of In/P ≈ (50 ± 1)/(50 ± 1) (Figure S5).

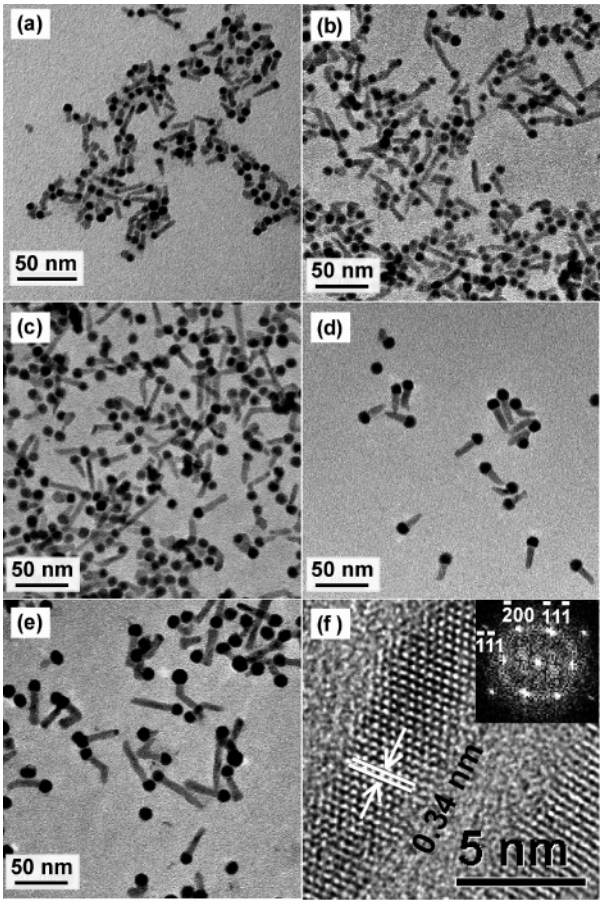

Figure 1. TEM images of InP QRs (mean diameter (d) by mean length (l)). (a) 4.8 nm × 16.2 nm, (b) 5.7 nm × 20.2 nm, (c) 6.3 nm × 17.1 nm, (d) 7.1 nm × 17.1 nm, and (e) 7.6 nm × 32.6 nm. (f) HRTEM image of a 4-nm-diameter rod viewed in a [011] zone axis. The measured d_{111} lattice spacing of 0.34 nm indexed to the zinc blende structure of bulk InP (d_{111} = 0.3388 nm). Inset: a fast Fourier transform of the image, indicating that the rod grows in the [111] orientation.

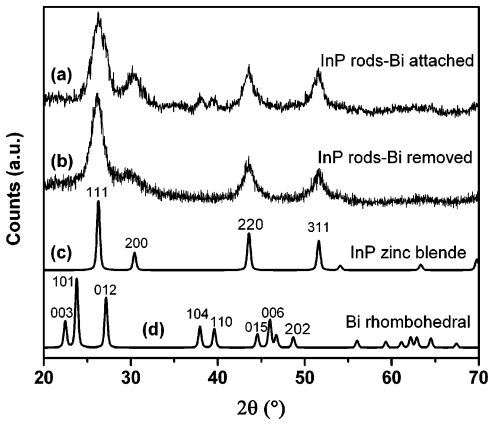

Figure 2. X-ray powder diffraction patterns for (a) as-prepared InP QR bulk specimens ($d \approx 6$ nm), (b) OA-etched InP QR bulk specimens ($d \approx 6$ nm), and (c) the simulated pattern for zinc blende (cubic) InP (ICDD PDF file 00-032-0452) and (d) for rhombohedral Bi (ICDD PDF file 00-044-1246).

Removal of the Bi Tips. A method was sought to remove the Bi tips by taking advantage of the reactivity difference of Bi and InP toward potential etching reagents. Very dilute

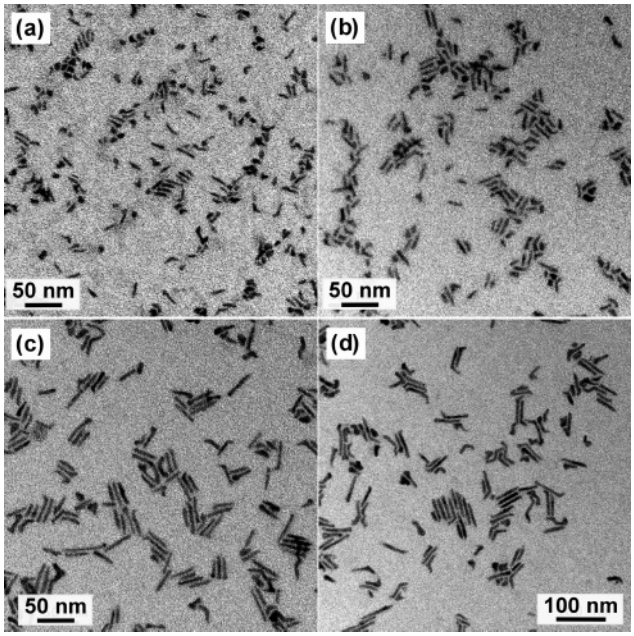

Figure 3. TEM images of InP QRs after the Bi tips were removed by OA etching ($d \times l$). (a) 4.0 nm × 12.5 nm, (b) 4.2 nm × 15.0 nm, (c) 4.5 nm × 24.8 nm, and (d) 7.1 nm × 31.6 nm.

hydrochloric acid was such a strong etchant that it dissolved both Bi and InP nanostructures. Carboxylic acids employed with sonication efficiently removed Bi while maintaining the intact InP QRs. However, the short-chain carboxylic acids such as acetic acid caused severe aggregation because of the poor resultant solubility of the etched QRs. Dispersibility was improved somewhat by using the long-chain myristic acid. However, well-dispersed InP QRs were achieved by using oleic acid (OA, Figure 3). After being etched with OA, residual Bi was undetectable by XRD (Figure 2b) and EDX (Figure S5). The small, irregularly shaped nanoparticles evident in Figure 3 are poorly formed rods, which were also present before Bi tip removal (Figure 1).

The diameters of the InP QRs were effectively thinned by the OA etching procedure, whereas the lengths remained unchanged or were longer (Tables S1 and S2). Presumably, the destruction of ultra-short QRs during etching and/or their separation in a length-selective precipitation process were responsible for increasing the fraction of long QRs in these etched samples. The OA-etched QRs had mean diameters of 3.8−7.4 nm and mean lengths of 10−42 nm. The standard deviations in the diameter distributions ranged from 11 to 18% of the mean diameter, and the standard deviations in the length distributions ranged from 26 to 42% of the mean length (see Figure S6 for representative size-distribution histograms). The length distributions were narrowed compared to those of the corresponding QRs before OA etching (Tables S1 and S2).

Surface Ligand Characterization. To investigate which ligands passivated the InP QRs, the QRs were carefully purified, the ligands were removed and recovered using a method adapted from Peng and Peng,[16] and the recovered ligands were then analyzed by TOF ESI MS.

For the as-prepared InP QRs containing Bi tips, only HDA (m/z = 242.3, positive mode) was detected by the ESI MS (Figure S7). Although TOPO, TOP, and myristate (from the indium precursor) were also used in the synthesis, none were

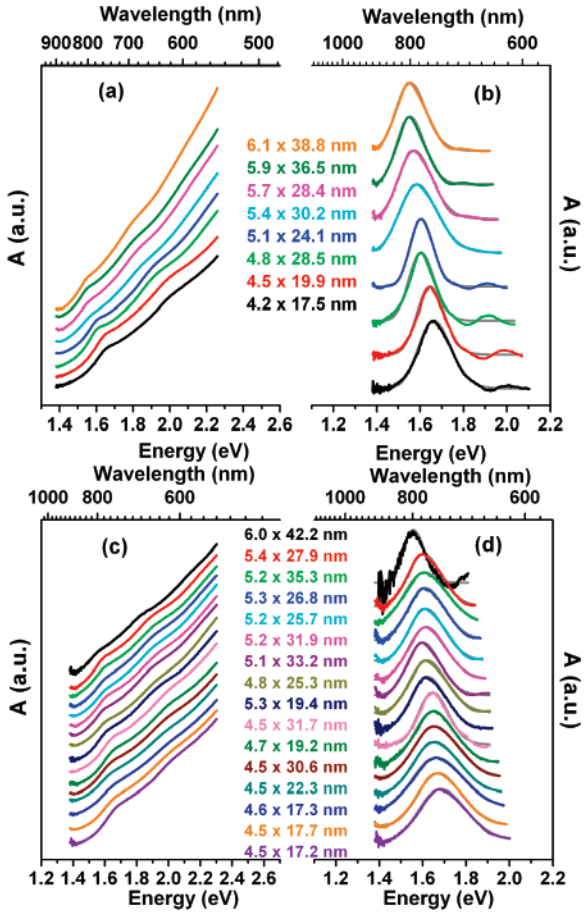

Figure 4. Representative absorption spectra of as-prepared InP QRs (a) and InP QRs after the Bi tips were removed by OA etching (c); and corresponding lowest-energy excitonic peaks (b and d) extracted by nonlinear least-squares fitting and background subtraction (various colors), and the Gaussian fits to those peaks (gray). Rod diameters (d values) and lengths (l values) are given in the keys ($d \times l$).

detected by either positive- or negative-mode ESI MS. This study showed that the InP QRs were passivated only by HDA. This is comparable to a similar study of the surface ligands for InP QWs,[29] in which we found a predominant amount of HDA and only small amounts of TOPO and myristate.

For OA-etched InP QRs, HDA (m/z = 242.3), TOPO (m/z = 387.4), and *N*-hexadecyltetradecanamide (m/z = 452.5) were identified by the positive-mode ESI MS (Figure S8). However, their ratios were not investigated. *N*-Hexadecyltetradecanamide is a condensation product of HDA and myristic acid. The presence of TOPO and *N*-hexadecyltetradecanamide could result from the incompletely purified InP QRs used for OA etching. Apparently, the InP QRs became partially passivated by TOPO and *N*-hexadecyltetradecanamide in the OA etching process. Many other peaks were present, among which OA (m/z = 283.5, positive mode) could not be identified, even in the negative mode (m/z = 281.5).

Absorption Spectroscopy. The QR band gaps were estimated from the lowest-energy exciton features in the absorption spectra (Figure 4a,c).[30] Each spectrum showed two excitonic peaks, which were broader than the corresponding peaks in the QD

(30) Yu, H.; Li, J.; Loomis, R. A.; Wang, L.-W.; Buhro, W. E. *Nat. Mater.* **2003**, *2*, 517−520.

absorption spectra reported previously.[27,31−36] The peaks in the QD spectra were sharper and better resolved because the size distributions of the dot specimens were narrower (size distributions about ±8−10%)[31−33,36] than those of the QR specimens reported here. The peaks in QR spectra were sharper than those in quantum wire spectra (size distributions about ±13−21%)[29,30] because of the narrower diameter distributions in QR specimens. To determine the band gap energies of the QRs, the absorption spectra in Figure 4a,c were empirically fit and the backgrounds subtracted using commercial nonlinear least-squares fitting software. The lowest-energy features in the resulting background-subtracted spectra (Figure 4b,d) were fit with Gaussian functions, and the band gap energies were assigned as the centers of Gaussian peaks (Tables S1 and S2). ΔE_g values were calculated as the increases in the band gap energy over the bulk value for InP (1.35 eV at 298 K).

Recent results have shown that the lowest-energy excitonic peak of InP QDs was red-shifted after the growth of metallic indium islands on the QD surface.[37] Comparison of the absorption spectra for InP QRs of like diameter and length with and without Bi tips would distinguish whether the Bi tips could affect the absorption properties of QRs. The QRs (without Bi) of 5.4 (*d*) nm × 27.9 (*l*) nm had the band gap energy of 1.60 ± 0.01 eV, whereas the QRs (with Bi) of 5.4 nm × (27.5−28.1) nm had the similar band gap energies of (1.59−1.60) ± 0.01 eV, demonstrating that the Bi tips did not influence the absorption spectra of InP QRs. This will be considered further in the Discussion.

Fluorescence Spectroscopy. The as-prepared InP QRs did not show detectable room temperature PL, which is not surprising in comparison to the PL from InP QDs. To the best of our knowledge, the PL quantum yield (QY) for the as-grown InP QDs was normally lower than 0.2%,[27,35,36] although it could reach 2% for those synthesized in a noncoordinating solvent.[20,38] The PL QY was further enhanced by etching the InP QDs with fluoride compounds (i.e., HF).[31−34] The reproducibility and reliability of the etching procedure was considerably improved by combining the HF treatment with photochemical irradiation.[27,36] The PL QYs for InP QDs of 40% have now been reported.

We adapted this photochemical etching technique to InP QRs. Figure 5a shows representative room temperature absorption and PL spectra of InP QRs after HF photochemical etching. As expected, the excitonic absorption peaks shifted to higher energy after etching, as the QR size decreased from 5.1 nm × 24.1 nm to 5.0 nm × 21.9 nm as measured by TEM. The PL QYs for InP QRs reached only 0.16%, perhaps because of the presence of Bi tips even after HF etching (Figure 5a, inset). The Bi tips

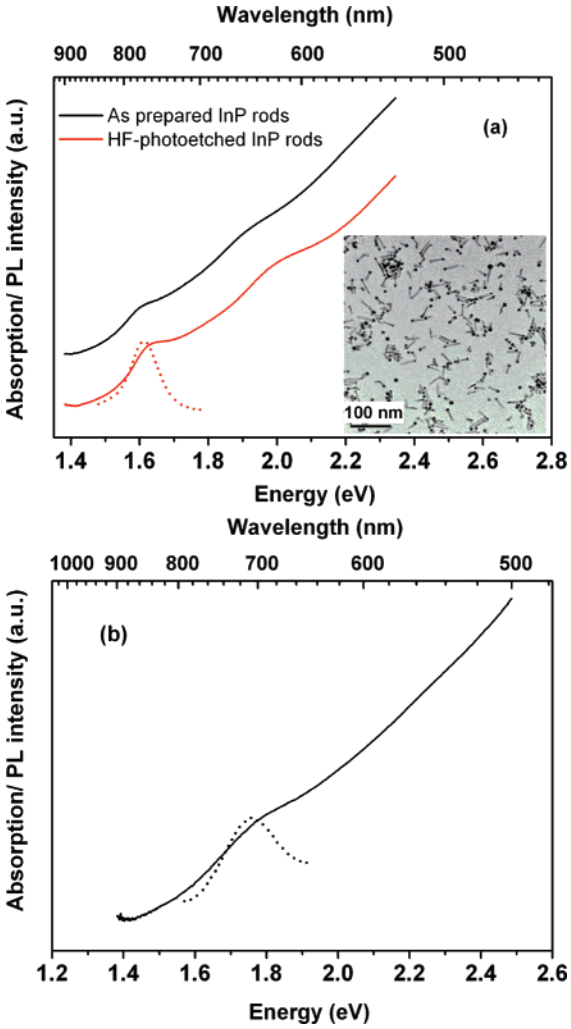

Figure 5. Representative PL (dotted line) and corresponding absorption (solid line) spectra. (a) InP QRs with Bi tips before (black, 5.1 nm × 24.1 nm) and after HF photoetching (red, 5.0 nm × 21.9 nm). Inset is the TEM image of InP QRs after etching. (b) InP QRs after the Bi tips were removed and after HF photoetching (4.2 nm × 12.6 nm). The samples in (a) and (b) are different.

could act as quenching centers to partially quench the PL, as has been demonstrated in Au/CdSe QRs,[39] Au/InP QRs,[37] and In/InP QDs.[37] In these cases, partial or complete PL quenching was ascribed to electron−hole separation to different locations in the heterostructures, which decreased the probability of their radiative recombination.[37,39] Therefore, we considered that removal of the Bi tips from the InP QRs may increase the PL QYs.

The OA-etched QRs exhibited very weak room temperature band-edge PL with a QY up to 0.05%. Further applying HF photochemical etching as described earlier enhanced the PL QYs up to 0.6%, much improved as compared with that when Bi tips were present (Figure 5b). To our knowledge, these results constitute the first report of PL QYs for III−V QRs. The low PL efficiency for InP QRs is not surprising when compared with that of single (0.01−1%)[40] or ensembles of InP wires (PL not detected at room temperature).[29] Previous work has shown that the PL QYs decrease in the order of QDs > short QRs >

(31) Mićić, O. I.; Cheong, H. M.; Fu, H.; Zunger, A.; Sprague, J. R.; Mascarenhas, A.; Nozik, A. J. *J. Phys. Chem. B* **1997**, *101*, 4904−4912.
(32) Mićić, O. I.; Sprague, J.; Lu, Z.; Nozik, A. J. *Appl. Phys. Lett.* **1996**, *68*, 3150−3152.
(33) Mićić, O. I.; Jones, K. M.; Cahill, A.; Nozik, A. J. *J. Phys. Chem. B* **1998**, *102*, 9791−9796.
(34) Mićić, O. I.; Ahrenkiel, S. P.; Nozik, A. J. *Appl. Phys. Lett.* **2001**, *78*, 4022−4024.
(35) Guzelian, A. A.; Katari, J. E. B.; Kadavanich, A. V.; Banin, U.; Hamad, K.; Juban, E.; Alivisatos, A. P.; Wolters, R. H.; Arnold, C. C.; Heath, J. R. *J. Phys. Chem.* **1996**, *100*, 7212−7219.
(36) Adam, S.; Talapin, D. V.; Borchert, H.; Lobo, A.; McGinley, C.; de Castro, A. R. B.; Haase, M.; Weller, H.; Möller, T. *J. Chem. Phys.* **2005**, *123*, 084706.
(37) Dimitrijević, N. M.; Rajh, T.; Ahrenkiel, S. P.; Nedeljković, J. M.; Mićić, O. I.; Nozik, A. J. *J. Phys. Chem. B* **2005**, *109*, 18243−18249.
(38) Lucey, D. W.; MacRae, D. J.; Furis, M.; Sahoo, Y.; Cartwright, A. N.; Prasad, P. N. *Chem. Mater.* **2005**, *17*, 3754−3762.
(39) Mokari, T.; Rothenberg, E.; Popov, I.; Costi, R.; Banin, U. *Science* **2004**, *304*, 1787−1790.
(40) van Vugt, L. K.; Veen, S. J.; Bakkers, E. P. A. M.; Roest, A. L.; Vanmaekelbergh, D. *J. Am. Chem. Soc.* **2005**, *127*, 12357−12362.

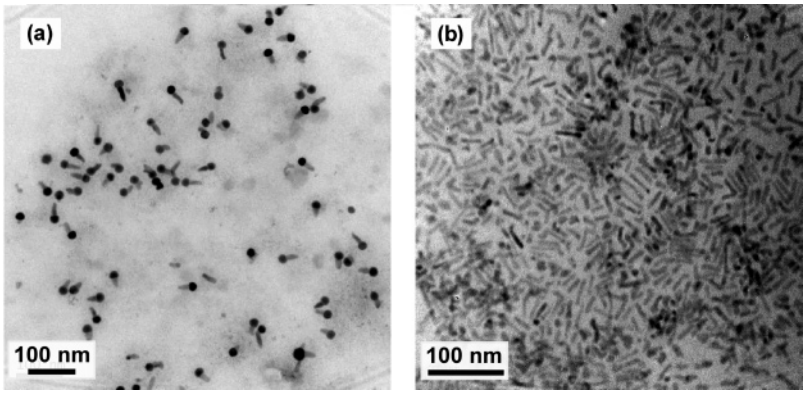

Figure 6. TEM images of InAs QRs grown from (a) Bi and (b) In nanoparticles.

medium QRs > long QRs > QWs[1,3,18,40] because of an increasing spatial separation of electron and hole wave functions and the increasing probability of surface carrier trapping.

Growth of InAs QRs. Diameter- and length-controlled InAs QRs were also grown from Bi nanoparticles by the SLS mechanism. Figure 6a shows a TEM image of InAs QRs synthesized from $In(myr)_3$ and $As(SiMe_3)_3$ in polydecene at 272 °C. Alternatively, InAs QRs were also grown from In nanoparticles at 250−300 °C (Figure 6b). The In atoms from the In nanoparticles were consumed during growth as the indium source, finally resulting in In nanoparticle-free InAs QRs, which were uniform and straight with well-controlled diameters and lengths.

Discussion

We previously argued that, to a rough first approximation, the quantum-confined band gap shifts ΔE_g in quantum wells, quantum wires, and quantum dots should all scale linearly with $1/d^2$, on the basis of an overly simple but intuitively attractive effective mass approximation, particle-in-a-box (EMA-PIB) model.[2,29,30] This EMA-PIB model compares the kinetic confinement energies of electrons and holes in various confinement geometries (dimensionalities) and led us to an approximate "rule of thumb" that in plots of ΔE_g vs $1/d^2$ for corresponding sets of QDs and QWs the ratios of the slopes should be $A_{wire}/A_{dot} = 0.585$.[2,29,30] We have experimentally compared the diameter dependencies of the band gaps of QWs and QDs in the InP[29,30] and CdSe[2] systems, and both comparisons were found to be consistent with the proposed rule of thumb. Such comparisons provide a picture of how quantum confinement scales with the geometric dimensionality of confinement.

As noted earlier, the anisotropic, 3D quantum confinement in QRs is intermediate to that in QDs and QWs; thus, the QR band gaps should be lower (higher) than those of QDs (QWs) of like diameter. In plots of ΔE_g vs $1/d^2$ for corresponding sets of QDs, QWs, and QRs, the QR values should fall in a rod zone between the dot and wire lines. The QR band gaps of short rods should tend toward the dot line, whereas those of long rods should tend toward the wire line. Obviously, QRs of intermediate length should have band gaps that fall in the middle of the rod zone. QRs having lengths sufficient to surpass the 3D−2D transition length should have band gaps that fall on the wire line.

The size dependencies of the band gaps in InP QRs are compared with those of InP QDs and QWs in Figure 7. ΔE_g values for InP QDs,[32−34] QRs (with Bi tips), and QWs[29] are plotted vs $1/d^2$ in Figure 7a. The purple points, corresponding to the short rods (l < 24 nm), are located above the wire line and within the rod zone; thus, these short rods behave optically as true QRs. All other rods in Figure 7a (blue points) fall on or very close to the wire line, some of which are in the 3D−2D transition regime from QRs to QWs. The long rods having similar diameters but different lengths were grouped together to determine the 3D−2D transition length within each group.

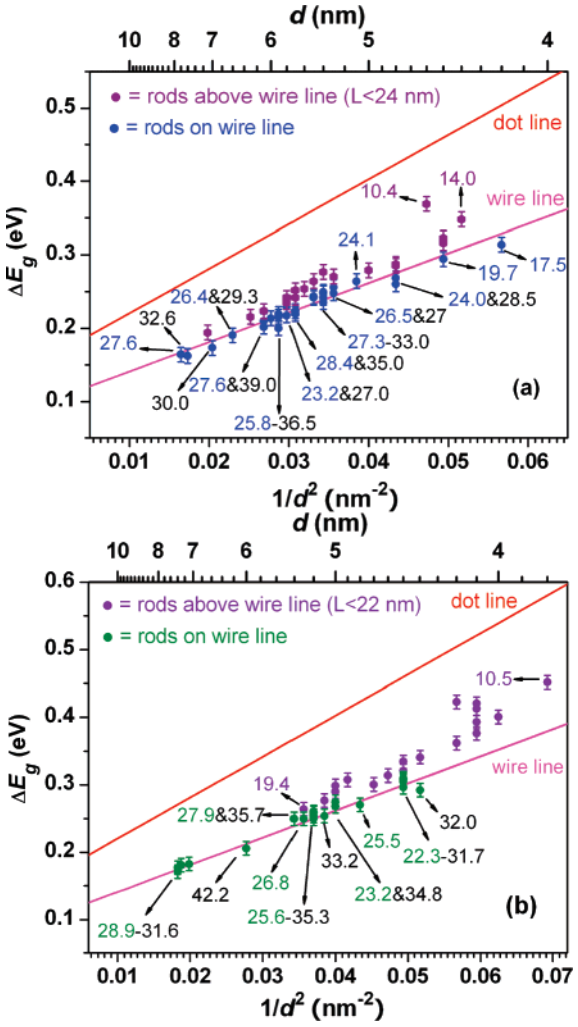

Figure 7. Plots of ΔE_g vs $1/d^2$. The red and pink lines are linear least-squares fits to InP QD[32−34] and QW[29] data, respectively. (a) Purple points correspond to InP QRs (with Bi) of l < 24 nm, and blue points to $l \geq 24$ nm. (b) Violet points correspond to InP QRs (without Bi) of l < 22 nm, and olive points to $l \geq 22$ nm.

In each diameter grouping, the longer of the long rods behave optically as true wires, whereas the shortest of the long rods, having lengths labeled with blue numbers (Figure 7a), are much closer to the rod-to-wire transition. The average of these blue, transition-length values is 24.8 nm, suggesting that an InP QR becomes a QW at lengths of ≥25 nm, or about twice the bulk InP exciton Bohr radius (of ∼11 nm).

As we have shown earlier that the Bi tips had no significant influence on the InP QR band gaps measured by absorption spectroscopy, one might anticipate that the Bi tips would not affect the calculated 3D−2D QR−QW transition length. Data for InP QRs after removal of the Bi tips are shown in Figure 7b. The violet points (l < 22 nm) in Figure 7b located above the wire line correspond to true QRs. The olive points labeled with olive numbers represent the rod-to-wire transition as described earlier. These olive numbers averaged to 25.7 nm, comparable to the transition length of 24.8 nm obtained earlier for InP QRs with intact Bi tips. Thus, the Bi tips did not affect the 3D−2D QR−QW transition length.

We have therefore found a 3D−2D QR−QW transition length in InP QRs of 25 nm, which is approximately twice the bulk exciton Bohr radius of 11 nm. This result provides an interesting contrast to the transition length determined similarly for CdSe QRs.[2] As noted earlier, the transition length in CdSe QRs was theoretically predicted to be about twice the exciton Bohr radius of 5.6 nm[5,6] but was found experimentally to be ≥30 nm, or about 6 times the Bohr radius.[2] We suspect that the discrepancy between the theoretical and experimental transition lengths may be due to the surfactant-controlled synthetic method employed for the CdSe QRs.[4,12−17.]

CdSe QRs prepared by surfactant-controlled growth often contain diameter fluctuations and other irregularities. A recent STEM study conducted by Krauss and co-workers found random, small-angle crystallographic twists and bends in different segments of CdSe QRs obtained in this manner and suggested that an attachment and coalescence mechanism may have contributed to their growth.[41] Experimental[42] and theoretical[43] studies have established that diameter fluctuations in quantum wires can induce exciton localization and dotlike emission from the resulting localized domains. Consequently, the larger experimental 3D−2D transition length in the CdSe QRs may reflect the increased overall length necessary to produce average localized domains having lengths of twice the bulk exciton Bohr radius (11.2 nm). Although imperfections are also clearly evident in the InP QRs grown by the SLS method (Figures 1 and 3), these may be crystallographically more uniform and closer to single crystal in character because of the different, catalyst droplet-mediated growth mechanism.

Conclusion

We have grown soluble, narrowly dispersed InP QRs with controlled diameters and lengths by the SLS mechanism in the presence of conventional QD surfactants. QRs that were photochemically etched in the presence of HF exhibited band-edge PL, with QYs of up to 0.6% after the Bi tips were removed. Comparisons between QRs with and without Bi tips showed that the Bi tips did not affect the absorption properties of InP QRs and the rod−wire transition length. The 3D−2D QR−QW transition length in the InP QRs was determined to be 25 nm, which is about 2 times the bulk InP exciton Bohr radius (of ∼11 nm).

Acknowledgment. We thank Prof. Richard A. Loomis and Dr. Lin-Wang Wang for helpful discussions. We are grateful to the National Science Foundation for funding this work under Grant No. CHE-0518427.

Supporting Information Available: Additional methods (TEM, XRD, absorption and fluorescence spectroscopy, surface-ligand characterizations, and syntheses of Bi nanoparticles and InAs QRs), tables listing detailed synthetic conditions, enlargements of Figures 1a and 3c, diameter and length distribution histograms of InP QRs, a plot of InP QR diameter as a function of the initial Bi catalyst nanoparticle diameter, HRTEM images of InP QRs having twinning defects, EDX spectra for as-prepared and OA-etched InP QRs, and mass spectra of the surface ligands for as-prepared and OA-etched InP QRs. This material is available free of charge via the Internet at http://pubs.acs.org.

JA075015C

(41) Yu, Z.; Hahn, M. A.; Calcines, J.; Krauss, T. D.; Silcox, J. *Appl. Phys. Lett.* **2005**, *86*, 013101.
(42) Hasen, J.; Pfeiffer, L. N.; Pinczuk, A.; He, S.; West, K. W.; Dennis, B. S. *Nature* **1997**, *390*, 54−57.
(43) Zhao, Z.; Wang, L.-W.; Wu, F. *J. Theor. Comput. Nanosci.* **2007**, *4*, 247−251.